The American Journal of Human Genetics, Volume *110*

Supplemental information

Stretch-activated ion channel TMEM63B associates with developmental and epileptic encephalopathies and progressive neurodegeneration

Annalisa Vetro, Cristiana Pelorosso, Simona Balestrini, Alessio Masi, Sophie Hambleton, Emanuela Argilli, Valerio Conti, Simone Giubbolini, Rebekah Barrick, Gaber Bergant, Karin Writzl, Emilia K. Bijlsma, Theresa Brunet, Pilar Cacheiro, Davide Mei, Anita Devlin, Mariëtte J.V. Hoffer, Keren Machol, Guido Mannaioni, Masamune Sakamoto, Manoj P. Menezes, Thomas Courtin, Elliott Sherr, Riccardo Parra, Ruth Richardson, Tony Roscioli, Marcello Scala, Celina von Stülpnagel, Damian Smedley, TMEM63B collaborators, The Genomics England Research Consortium, Annalaura Torella, Jun Tohyama, Reiko Koichihara, Keisuke Hamada, Kazuhiro Ogata, Takashi Suzuki, Atsushi Sugie, Jasper J. van der Smagt, Koen van Gassen, Stephanie Valence, Emma Vittery, Stephen Malone, Mitsuhiro Kato, Naomichi Matsumoto, Gian Michele Ratto, and Renzo Guerrini

Supplemental information

Sections:

Supplemental Materials and Methods

MRI investigations

All individuals underwent standard brain magnetic resonance imaging (MRI) as part of their routine clinical care. Ten out of 17 individuals were imaged at least twice. Data were acquired using 1.5-T or 3-T systems, with T1-weighted, T2-weighted, and fluid attenuated inversion recovery (FLAIR) sequences in axial, sagittal, and coronal planes at the respective centers.

Genetic investigations

We performed whole exome (WES, IDs 1-3, 5, and 8-17) and genome (WGS, IDs 4 and 6) sequencing using standard procedures on DNA extracted from peripheral blood. In all but IDs 7 and 10, whose DNA was sequenced as singleton, we used a patient-parent trio sequencing strategy. We prepared DNA libraries by different kits according to manufacturers' instructions and performed paired-end sequencing on Illumina sequencers (Illumina, San Diego, CA, USA). We aligned sequencing reads to the human reference genome build GRCh37/hg19 by the Burrows-Wheeler Alignment (BWA-MEM) software package[1] and followed the Genome Analysis Toolkit Best Practices workflow[2] for variant calling. Detailed sequencing and variant annotation methods for each individual are provided as a reference to previous publications in the Supplementary Table 4. For variant analysis, we focused on exonic/splice-site single-nucleotide variants (SNVs) and coding insertions/deletions (InDels) with minor allele frequency (MAF) lower than 0.01 in the GnomAD v2.1 (http://gnomad.broadinstitute.org/)[3] or TOPMed (https://bravo.sph.umich.edu/freeze3a/hg19/) datasets. We excluded population-specific variants by interrogating our internal database (singleton WES data from approximately 2000 individuals with DEE). We evaluated the potential impact of SNVs and InDels by the pre-computed genomic variants score from dbNSFP[4] and by the evolutionary conservation scores.[5,6] After filtering and interpretation, we proceeded to validation of the *TMEM63B* variants by Sanger sequencing (primers and conditions available on request). We followed the nomenclature guidelines of the Human Genome Variation Society (HGVS, http://www.hgvs.org/mutnomen) and referred to the NM_018426.3 reference transcript.

We evaluated *TMEM63B* gene-level constraint scores according to GnomAD[3] and the region-level constraint scores according to the Metadome and MTR tools.[7,8]

Homology modelling and structural analysis

To evaluate the evolutionary conservation of the mutated residues, we obtained the protein sequence of human TMEM63B, its paralogues TMEM63A and TMEM63C, and orthologues in five different vertebrate species (*Pan troglodytes, Sus scrofa, Mus musculus, Gallus gallus, Danio rerio*) from the NCBI Protein Database,[9] and aligned them using Clustal Omega.[10] As the protein crystal structure of TMEM63B has not been determined, we used the protein homology recognition engine Phyre2[11] to predict and analyse the protein structure. For structural modelling, we referred to the NP_060896.1 human TMEM63B protein sequence using the Phyre2 'intensive mode' prediction option. To further analyse possible effects of the recurrent p.Val44Met, we calculated the free energy change due to this substitution by the FoldX software[12,13] using a TMEM63B structural model predicted by AlphaFold2.[14] We also generated a tridimensional model incorporating evolutionary sequence conservation with the ConSurf webserver[15] with default parameters. We used the Missense3D tool[16] to predict possible structural changes introduced by the missense substitutions. To graphically represent the variants identified in our individuals on the homology-predicted protein model we used the UCSF Chimera Visualization System.[17]

RNA reverse transcription and cDNA analyses

We reverse-transcribed total RNA from healthy adult human cerebral cortex (BioChain, Newark, USA) into cDNA using the High-Capacity RNA-to-cDNA Kit (Applied Biosystems, Waltham, USA). We performed polymerase chain reaction (PCR) on the cDNA using the FastStart Taq DNA Polymerase (Roche, Basel, Switzerland) and *TMEM63B* primers designed with the Primer3 Plus software (https://www.bioinformatics.nl/cgi-bin/primer3plus/primer3plus.cgi) using the NM_018426.3 transcript as template. Primers and RT-PCR conditions are available upon request.

To characterise the alternative splicing of exon 4 in the *TMEM63B*, we amplified the cDNA region spanning the exon 4 (exons 3-8) and analysed the PCR product by agarose gel electrophoresis. We acquired the gel images by ChemiDoc Imaging System (Bio-Rad, Hercules, USA) and quantified the two cDNA bands we resolved by ImageJ software (National Institutes of Health, USA). We quantified the expression level of the two isoforms as the ratio of integrated densities of the two bands to the total. We extracted the cDNAs from

excised gel bands (Macherey-Nagel, Düren, Germany), sequenced them and analysed the electropherograms using the SnapGene software (https://www.snapgene.com/) to confirm that they corresponded to the two *TMEM63B* isoforms with (herein referred to as "long" isoform) or without (herein referred to as "short" isoform) exon 4. As an orthogonal method to confirm the relative expression level of both isoforms, we also cloned the PCR product in TOPO TA cloning (Invitrogen, Waltham, USA) and used Sanger Sequencing to determine the number of colonies containing the long or the short isoform.

To characterise the Q/R editing at exon 20 in the *TMEM63B*, we amplified the cDNA region including exon 20 in both isoforms. To quantify the editing occurrence in both isoforms, we cloned the PCR products in TOPO TA cloning and counted the number of colonies containing the editing.

TMEM63B constructs

We designed wild type (WT) and mutant (p.Arg325*, p.Val44Met, p.Arg433His, p.Thr481Asn, p.Gly580Ser, p.Arg660Thr, and p.Phe697Leu) human *TMEM63B* cDNAs corresponding to the most represented isoform in the human cerebral cortex (short not edited), with the hemagglutinin (HA) tag sequence (AGCGTAATCTGGAACATCGTATGGGTA) at the 5' end. We obtained *TMEM63B* cDNAs and cloned them into the pGP-CMV-GCaMP6f vector (Plasmid #40755, Addgene, Watertown, USA),[18] so that the cDNA is fused to the N-terminus of GCaMP6f via a P2A linker forming a tandem expression system (TMEM63B-P2A-GCaMP6f) (Genescript, Piscataway, USA). The correct orientation and sequence of the cDNAs were checked by Sanger sequencing by Genescript.

Cell culture and transfection

We maintained Neuro2A mouse neuroblastoma cells at 37°C in a humidified 5% CO_2 incubator in Dulbecco's Modified Eagle Medium (Invitrogen, Waltham, USA) supplemented with 10% foetal bovine serum (FBS) and 2 mM L-glutamine. For the electrophysiology experiments, we plated the cells onto 13 mm square glass poly-L-lysine coated coverslips. The cells used in the Ca-imaging experiments were plated on WillCo Wells dishes HBST-3512 (WillCo Wells B.V., Amsterdam, The Netherlands). We transfected Neuro2A cells using Lipofectamine 2000 (Invitrogen) according to manufacturer's instruction.

Immunocytochemistry and confocal microscopy

Forty-eight hours post transfection, we fixed Neuro2A cells in 4% paraformaldehyde in phosphate-buffered saline (PBS) for 15 minutes at room temperature, blocked with 10% normal goat serum and 0.1% bovine serum albumin (BSA) in PBS for one hour at room temperature and incubated in 0.1% BSA in PBS overnight at 4°C with the primary anti-HA tag antibody (1:500, #2367, Cell Signaling Technology, Inc., Danvers, USA). After washing in PBS, we incubated the cells in 0.1% BSA in PBS for one hour at room temperature with the secondary Alexa Fluor 555 antibody (1:500, #A21424, Thermo Fisher Scientific, Waltham, USA). We washed the cells in PBS and mounted coverslips with ProLong Gold Antifade Mountant with DAPI (#P36935, Thermo-Fisher Scientific). We acquired images of 100 x 100 µm area using a laser scanning confocal microscope (SP5, Leica, Wetzlar, Germany) and analysed data with ImageJ software (National Institutes of Health, Bethesda, USA).

In *Drosophila*, we performed immunohistochemistry and sample preparation as described previously.[19] Briefly, we dissected the adult fly brains in PBS, fixed them in 4% formaldehyde (Electron Microscopy Sciences, USA), and incubated the samples with mouse anti-myc (4A6; 1:5000; Merck KGaA, Darmstadt, Germany) and secondary anti-mouse Alexa Fluor 568 (1:400; Thermo Fisher Scientific). We acquired images using a FV3000 confocal microscope (Olympus, Tokyo, Japan), and processed and analysed them using IMARIS 9.6.0 (Bitplane, Zurich, Switzerland).

Electrophysiology

Forty-eight hours post transfection, we recorded Neuro2A cells by whole-cell patch clamp. Recording pipettes were obtained from borosilicate capillaries (Harvard Apparatus, Holliston, USA) with a Narishige vertical puller (Narishige, Tokyo, Japan) and back-filled with a solution containing (in mM) 80 K-gluconate, 10 HEPES, 130 Mannitol (pH 7.4 with KOH, 300 mOsm/L), resulting in a bath resistance of 8-10 MΩ. We initially perfused cells with an isotonic extracellular solution containing (in mM): 80 Na-gluconate, 1 Ca-gluconate, 10 HEPES, 130 Mannitol (pH 7.4 with NaOH, 300 mOsm/L) at room temperature and with a flow rate of approximately 1 ml/min. The hypo-osmotic extracellular solution contained (in mM): 80 Na-gluconate, 1 Ca-gluconate and 10 HEPES (pH 7.4 with NaOH, 170 mOsm/L). The osmolarity of the solutions used in both patch clamp and calcium imaging experiments was measured by an osmometer (OSMOMAT 030,

Gonotec Gmbh, Berlin, Germany). Solutions were exchanged with an eight-line valve switcher (Hamilton Company, Reno, USA). We stimulated the cells with a voltage clamp protocol consisting of a 40 ms negative step to -80 mV, followed by a 100 ms ramp stimulus to +80 mV, imposed every 10 seconds. Holding potential was 0 mV. Signals were sampled at 10 kHz and low pass filtered at 3 kHz with an Axon Multiclamp 700B (Molecular Devices, Sunnyvale, USA). We performed data analysis offline with Clampfit 10 (Molecular Devices) and GraphPad 8.0 software (GraphPad, San Diego, USA).

Calcium imaging

Forty-eight hours post transfection, we acquired cells imaging with a ZEISS LSM800 Airyscan inverted microscope (ZEISS, Jena, Germany) at a resolution of 512x512 pixels (objective ZEISS ECPlan-NEOFLUAR 20x) with the standard settings for excitation and acquisition of Fluorescein (excitation 488nm, emission >500nm) at 0.5 Hz frequency for 600 seconds. During imaging, cells were exposed to solutions of variable osmolarity by perfusing the imaging chamber with peristaltic pumps (flux 1ml/min). The hypo-osmotic solution contained (mM): 65 NaCl, 5 KCl, 1 $CaCl_2$ 2, 1 $MgCl_2$ 2, 10 HEPES, pH=7.4, adjusted with NaOH. We prepared the isotonic solution adding mannitol to the hypo-osmotic solution to a final concentration of mannitol 130 mM without changing other ion concentrations.

Analysis of calcium imaging data

We analysed the acquired images with Fiji ImageJ software. For each field of acquisition, we generated an average projection, and we selected the cells which florescence was in the upper 95 percentile to exclude autofluorescent cells. We then analysed the selected cells by computing the fractional change of fluorescence defined as:

$$\Delta F(t) = \frac{F(t) - F_0}{F_0}$$

where F_0 indicates the baseline fluorescence computed as the average of the first 20 frames of the sequence. Cells were considered responsive when they presented changes of fluorescence larger than 50% of the baseline level.

Statistical analysis

We used the GraphPad 8.0 software for statistical analyses. We assessed the normal distribution of experimental data using the D'Agostino-Pearson normality test. We analysed data with normal distribution with One-way ANOVA followed by Tukey's multiple comparison test, while for non-normally distributed data we used the unpaired Mann-Whitney U test or Kruskal-Wallis test followed by Dunn's multiple comparison test. We set significance level at $p<0.05$ and expressed data as mean ± standard error of the mean (SEM).

For statistical analysis of calcium imaging, we used the Origin 2019b package (OriginLab, Massachusetts, USA). Hypotheses were tested with Mann-Whitney non-parametric tests. We considered results to be significant for $p<0.05$.

Drosophila strains and generation of the transgenic lines expressing human *TMEM63B* WT, p.Val44Met, and p.Gly580Cys

Flies were maintained at 25°C on standard fly food. *GMR-Gal4* (#1104) and *c739-Gal4* with *UAS-CD8GFP* (#64305) were obtained from the BDRC (Bloomington, Indiana, USA). *40D-UAS* (#60101) for control experiments was purchased from VDRC (Vienna, Austria). To express human TMEM63B WT, p.Val44Met, and p.Gly580Cys, tagged with Myc at C terminal of the protein, the cDNAs were inserted into pJFRC81-10XUAS-IVS-Syn21-GFP-p10 (ID36432, Addgene, Massachusetts, USA) (Vectorbuilder Inc., Yokohama, Japan). We used the phiC31 integrase system[20] to insert the transgenes in the same position of the fly genome and exclude potential positional effects on gene expression. These vectors were inserted into the *aTTP40* landing site (WellGenetics, Taipei, Taiwan). As the expression level of the Gal4/UAS system increases in a temperature-dependent manner,[21] the transgenic flies were reared at different temperatures (18°, 20°, 25° and 29°C), to modulate the expression of the transgene.

Eye imaging with bright-field microscopy and the quantification of morphological defects in the retina

TMEM63B WT and each the two variants p.Val44Met and p.Gly580Cys were expressed by the *GMR-Gal4* driver and reared at 20°C. One-day-old flies were immobilized by freezing at -80°C for imaging. These flies

were imaged using a BX53 microscope system with a MPLFLN 20x objective lens (Olympus, Tokyo, Japan). The phenotypic scores were calculated using Flynotyper.[22] Experimental analyses were performed using Prism 9 (GraphPad Software Inc., San Diego, CA, USA). The distribution of our data was determined using the D'Agostino & Pearson test and the Kolmogorov-Smirnov test (normality test was passed if $p > 0.05$). For data following a Gaussian distribution, we used ordinary one-way ANOVA with Tukey's multiple comparisons between groups.

Supplemental Figures

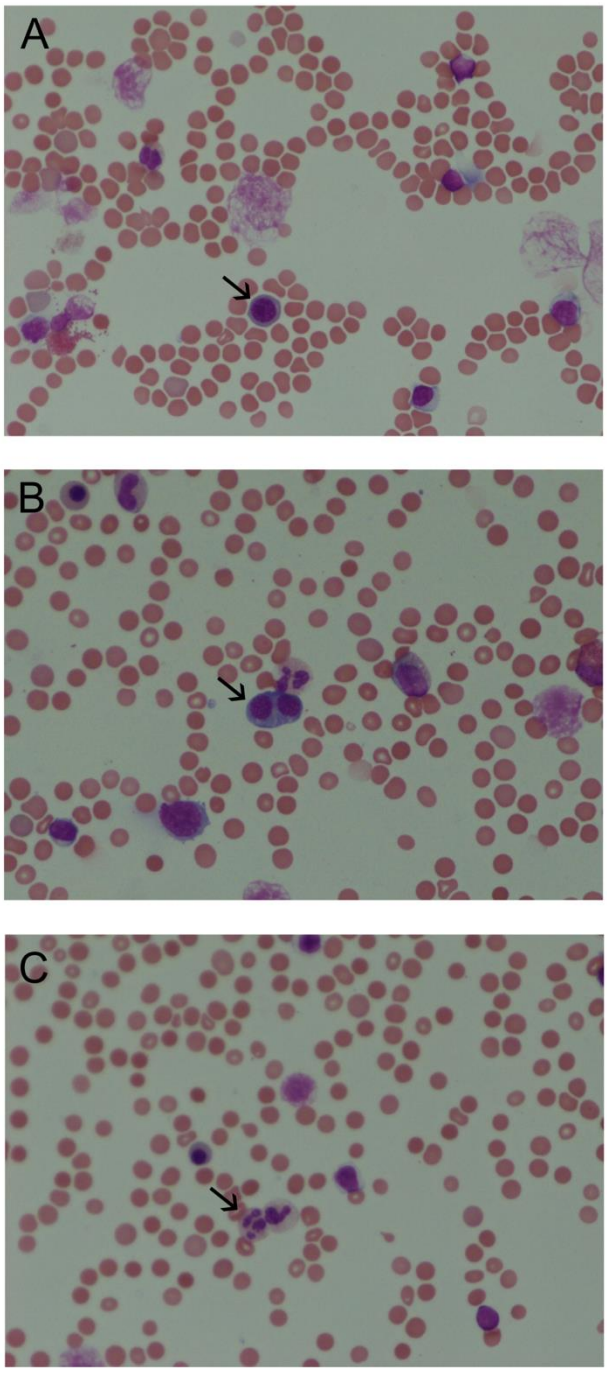

Figure S1 – Bone marrow aspirate smear from Individual 8

Bone-marrow examination in Individual 8 (age 8 years) revealed hypocellular marrow, signs of haemolysis, and evidence for haematopoiesis and myelodysplastic syndrome with aplastic anaemia. Arrows highlight examples of megaloblastic changes (A), binucleated erythroblasts (B), and Pseudo-Pelger–Huët anomalies (C) observed in the sample.

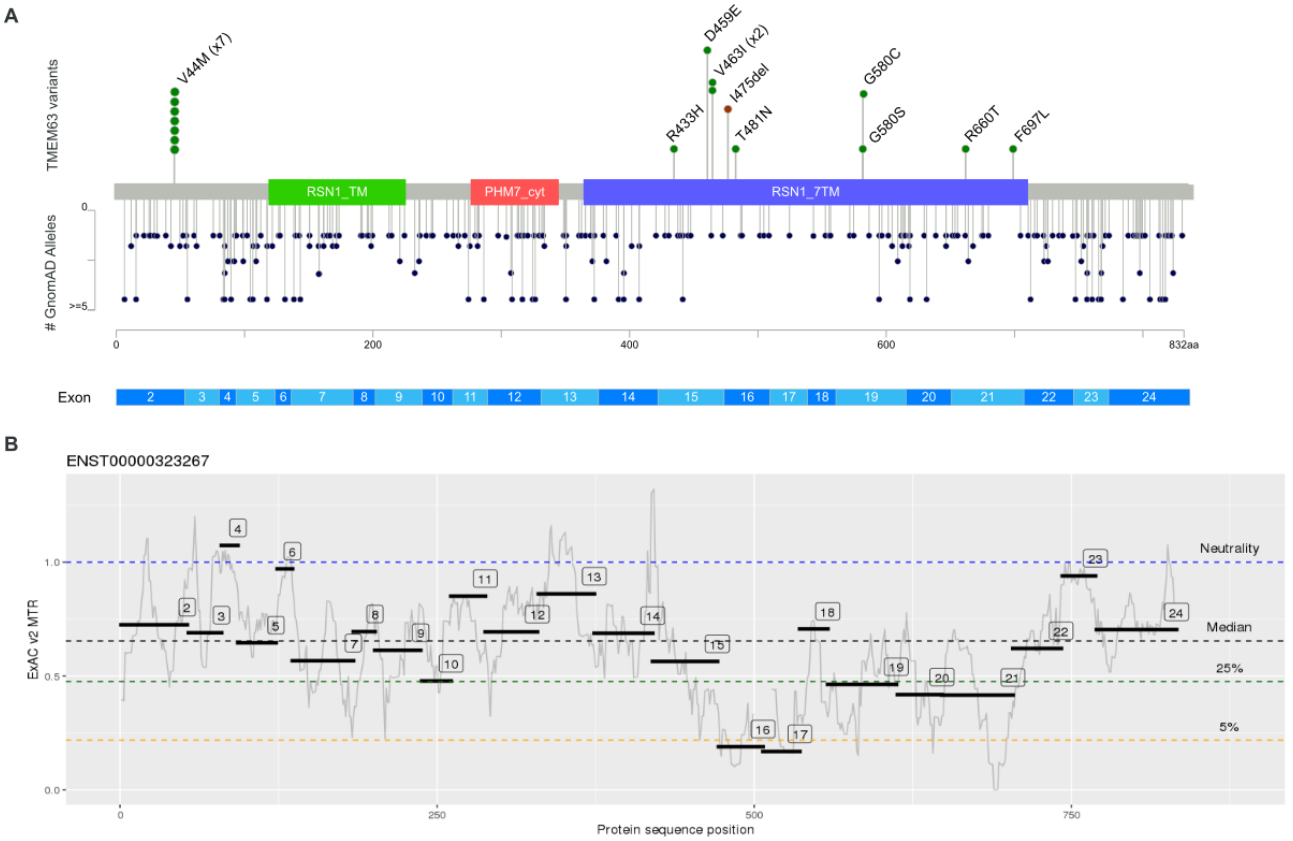

Figure S2 - Distribution of *TMEM63B* variants in our cohort and in reference population

(A) The lollipop diagram shows the distribution of the *TMEM63B* variants observed in our cohort (top, missense variants in green, in-frame deletion in brown) versus the reference population in GnomAD 2.1 (bottom, missense variants all in dark blue) on the linear protein map and relative to the Pfam-identified domains (RSN1_7TM, PF02714, green; PHM7_cyt, PF14703, red; RSN1_TM, PF13967, blue) of the protein and the *TMEM63B* exons (NM_018426.3, ENST00000323267). All but one of the *TMEM63B* variants in our cohort map in the RSN1_7TM domain (PF02714), which is conserved among osmosensitive calcium-permeable cation channels.[23] In the bottom panel, the length of the lollipop reflects the number of alleles in GnomAD 2.1 (see the Y-Axis on the left). The variants in our cohort maps in positions which are under constraint for missense variants. (B) The missense tolerance ratio (MTR)-Viewer tool[8] shows the local constraint with respect to the *TMEM63B* exons: all the variants in our cohort fall in regions where the MTR scores were below the neutrality threshold. The exon 16, bearing the T481N and the I475del variants, has the highest intolerance to missense substitutions, followed by the exons 15 (R433H, D459E, and V463I), 19 (G580S and G580C), 21 (R660T and F697L), and 2 (V44M).

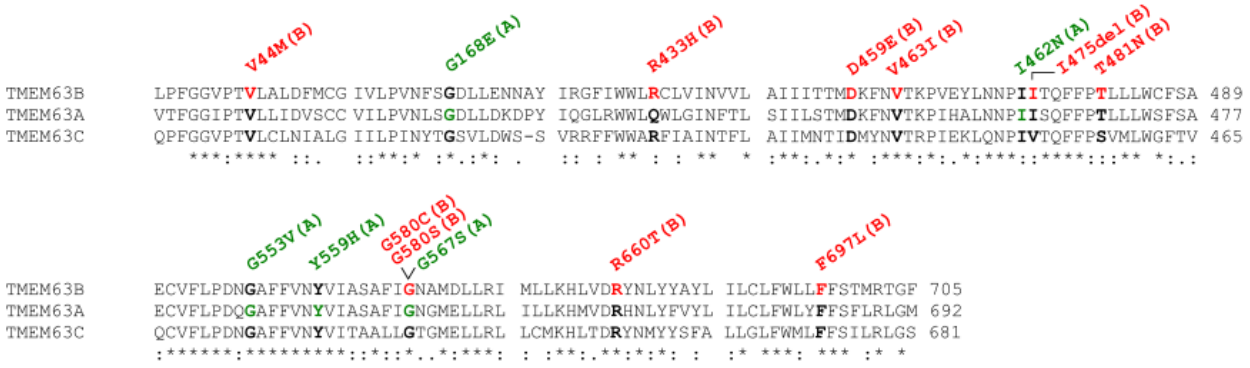

Figure S3 - Multiple sequence alignment of TMEM63A, B and C

The alignment shows the protein sequence of the human TMEM63B protein (NP_060896.1) and of its two paralogues TMEM63A (NP_055513.2) and TMEM63C (NP_065164.2). The residues affected by heterozygous variants of *TMEM63B* (our cohort, red) or *TMEM63A* (from the literature, green)[24–26] are in bold. The details of the variants are displayed above the alignments. The asterisk below the tracks indicates positions which have a single, fully conserved residue between all the input sequences, the colon indicates conservation between groups of strongly similar properties, and the period indicates conservation between groups of weakly similar properties. Six out ten *TMEM63B* variants in our cohort affected residues which are fully conserved among all the three paralogues' sequences (V44, D459, V463, G580, R660, and F697), and three affected residues conserved among two of the three paralogues and maintaining strongly similar properties in the other one (R443, T481 and I475).

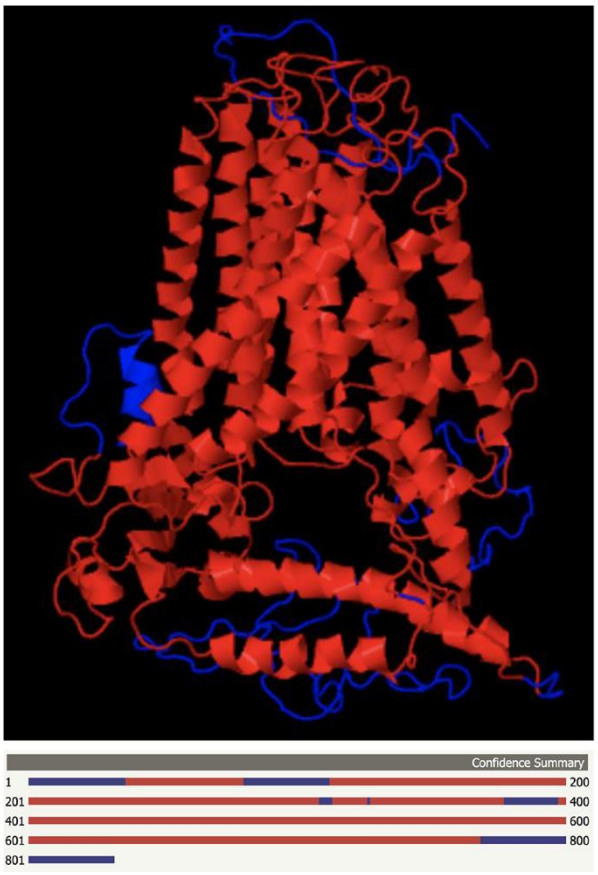

Figure S4 - Projection of confidence score for the TMEM63B protein structure

In the multi-template homology model obtained by Phyre2, the 81% of residues were modelled with >90% confidence and are showed in red both in the model (upper panel, side vision from the membrane plane) and in the confidence summary (lower panel, linear representation of the amino acids sequence), where low-confidence regions are in blue.

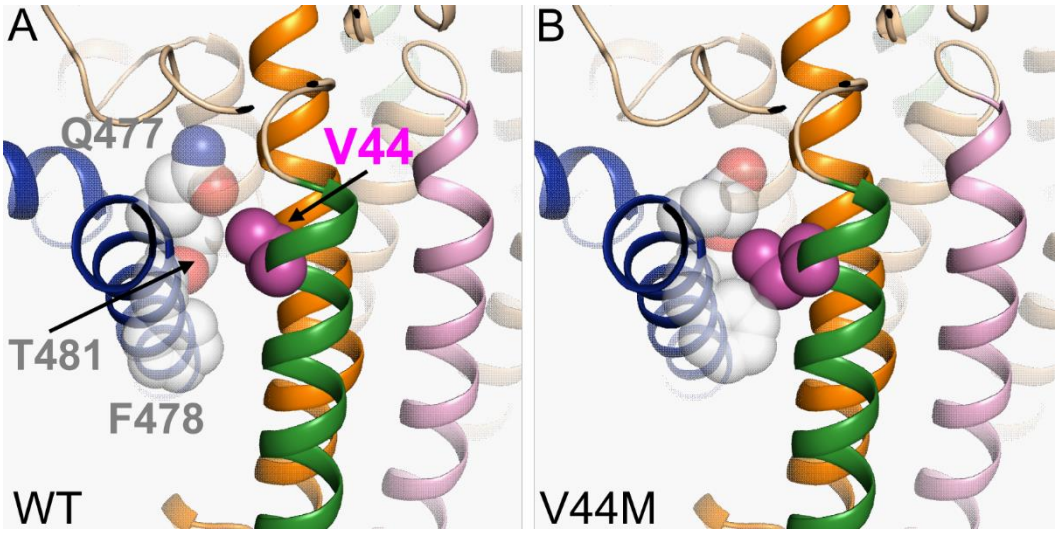

Figure S5 - Close-up of the protein region around Valine 44 in the WT and p.Val44Met TMEM63B

Transmembrane helices are colored as in Figure 3. V44 (purple) and the interacting residues G477, F478, and T481 are indicated by van der Waals spheres in the WT (A) and p.Val44Met mutated (B) model of the protein modeled by FoldX.

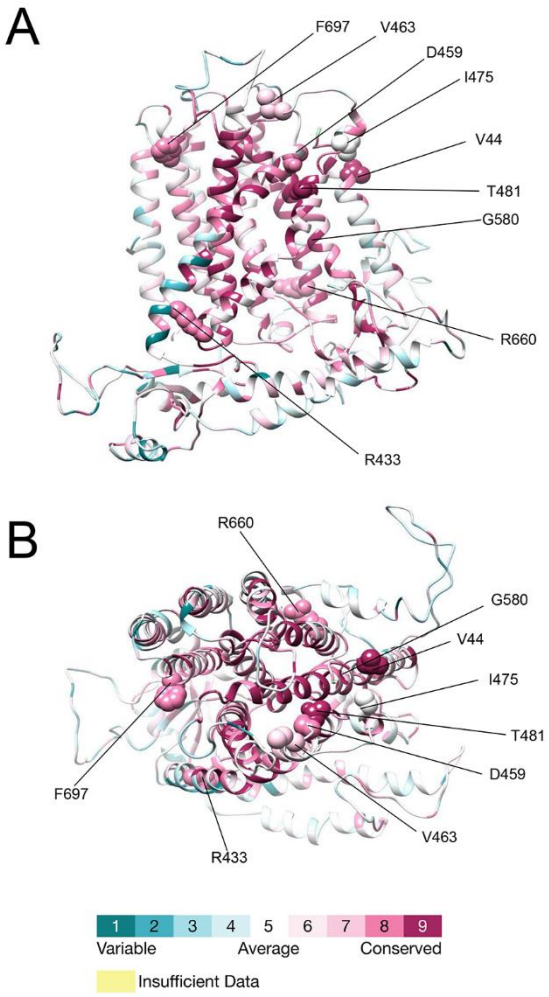

Figure S6 - ConSurf's projection of conservation scores onto the predicted structure of TMEM63B

View of the predicted structure of TMEM63B from the membrane plane (A) and the extracellular side (B). The color scale is dark aqua (least conserved) to dark magenta (most conserved). Detailed scored and prediction information for each of the residues affected by variants in our cohort are provided in Tables S2 and S3.

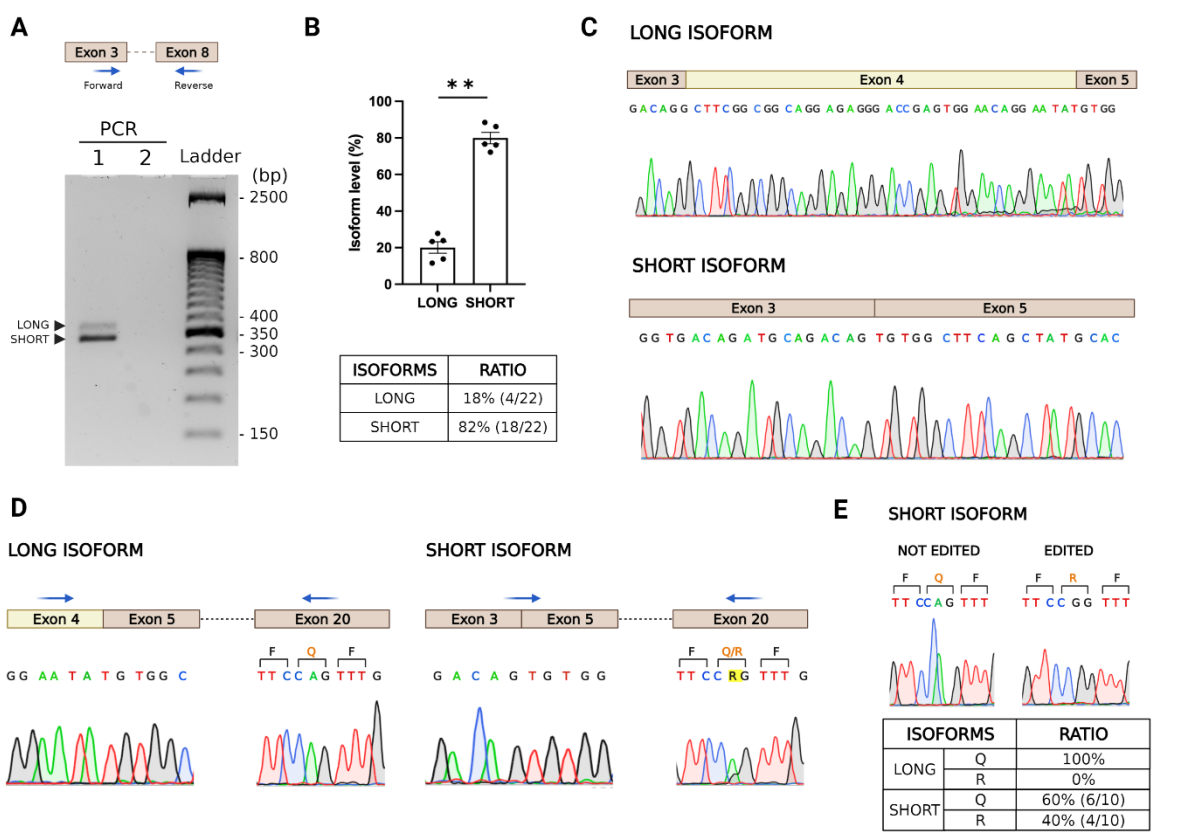

Figure S7 - Characterisation of alternative splicing of exon 4 and Q/R editing at exon 20 in *TMEM63B* RNA from human cerebral cortex

(A) Upper panel: schematic representation of *TMEM63B* exons 3-8 with arrows indicating Forward and Reverse primers for PCR amplification. Lower panel: agarose gel electrophoresis of the PCR products (Lane 1) showing both long and short *TMEM63B* isoforms, indicated by arrowheads. Lane 2, blank. (B) Upper panel: densitometric quantification of long and short isoforms from gel electrophoresis (data from 5 replicates, expressed as mean ± SEM. **p= 0.0079; Mann-Whitney U test). Lower panel: quantification of long and short isoforms levels obtained from TOPO TA cloning and subsequent sequencing of the PCR products expressed as the number of colonies containing the specific isoform over the total number of screened colonies. (C) Electropherograms from excised bands sequencing showing that exon 4 is only included in the long isoform. (D) Electropherograms of long and short isoforms showing exon 3-5 junctions and editing site at exon 20. A schematic representation of the corresponding exons is indicated, with blue arrows showing Forward and Reverse primers used for PCR amplification. For exon 20 the corresponding amino acids are reported above the nucleotide sequences at the editing site. (E) Upper panel: electropherograms of short edited and not edited isoforms showing the editing site at exon 20, obtained from TOPO TA cloning and subsequent sequencing of the short isoform PCR products. Lower panel: quantification of Q/R editing occurrence in long and short isoforms by TOPO TA technology. For each isoform, the percentage of editing occurrence is obtained from the ratio between the number of colonies edited (R) or not edited (Q) and the total number of analysed colonies.

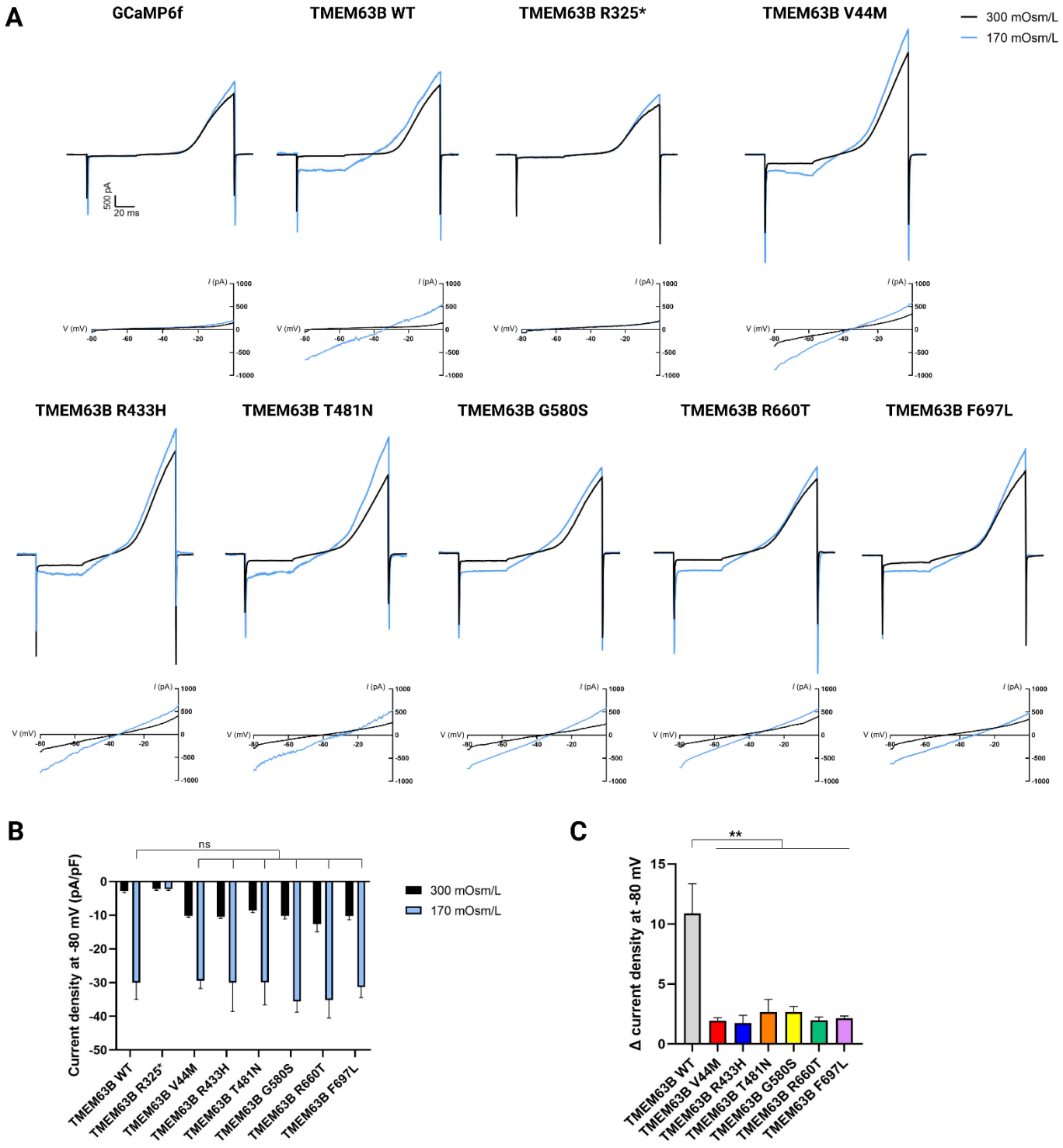

Figure S8 - Effect of hypo-osmotic stimulation on TMEM63B-mediated currents

(A) Representative current traces and current-voltage (I-V) relationships measured in Neuro2A cells transfected with GCaMP6f, TMEM63B WT or mutant plasmids and recorded with a -80 to + 80mV voltage ramp protocol in isotonic (300 mOsm/L) and hypo-osmotic (170 mOsm/L) conditions. (B) Quantification of whole-cell current density at -80 mV under isotonic and hypo-osmotic conditions (TMEM63B WT, R433H, T481N, G580S, and R660T = 6 cells, TMEM63B R325*, V44M, and F697L = 7 cells; ns = not significant,

Kruskal–Wallis and Dunn's multiple comparisons tests). (C) Quantification of the Δ current density measured at -80 mV between hypo-osmotic and isotonic conditions, calculated as:

$$\Delta \text{ current density at -80 mV} = \frac{(\text{hypo-osmotic current density}) - (\text{isotonic current density})}{(\text{isotonic current density})}$$

(TMEM63B WT, R433H, T481N, G580S, and R660T = 6 cells, TMEM63B V44M and F697L = 7 cells; **p<0.01, Kruskal–Wallis and Dunn's multiple comparisons tests). Data are expressed as mean ± SEM.

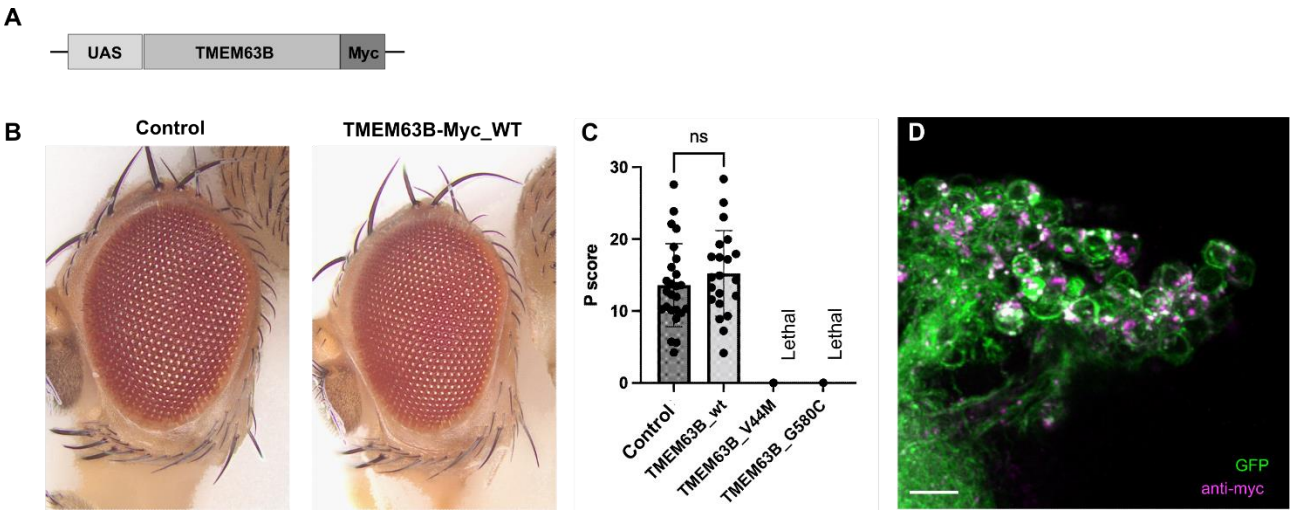

Figure S9 - Evaluation of human *TMEM63B* variants in *Drosophila*

(A) Cartoon depicting a *TMEM63B* gene construct with a Myc tag in UAS-based vector. (B) Representative bright-field microscope images of the eyes in control and WT TMEM63B-expressing flies (*GMR-Gal4* driver), and (C) quantification of the phenotypic scores in control ($n = 25$) and WT *TMEM63B* ($n = 21$), showing no significant differences in the eye morphology between the control and the WT *TMEM63B*-expressing flies. No data could be obtained for the V44M and G580C-expressing flies, as none of them reached the adult file stage. Data represent the mean ± SD (ns, not significant). (D) Three-dimensional projection of CD8:GFP-labeled Kenyon cells and myc-tagged WT TMEM63B in a posterior brain view in the adult stage. Scale bar = 10 μm.

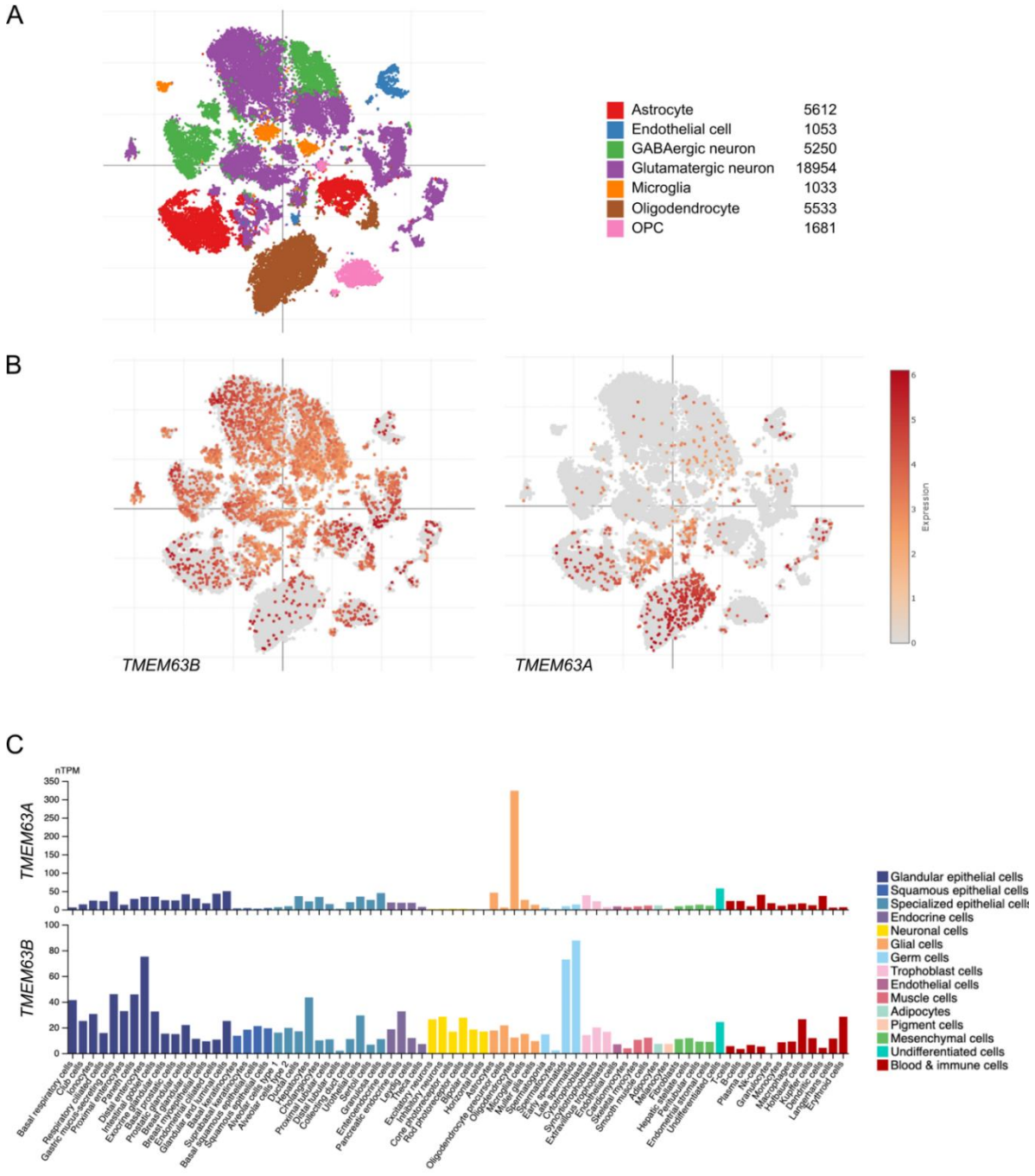

Figure S10 – Single-nucleus expression patterns of *TMEM63B* and *TMEM63A* in the human brain cortex

Panels A and B show the t-distributed stochastic neighbourhood embedding (tSNE) visualization of single-nucleus profiles (dots) coloured by cell type (A) and gene expression level (B). Single-nucleus RNA-seq data are shown according to the Single Cell Portal (https://singlecell.broadinstitute.org/single_cell/study/SCP381/).[27] (C) A summary of single cell RNA expression levels of *TMEM63A* and *B* as presented in the Human Protein Atlas (https://www.proteinatlas.org/). Color-coding is based on cell type groups (detailed on the right), each consisting of cell types with functional features in common. Abbreviations: pTPM, transcripts per million.

Supplemental Tables

Table S1 – Methods for exome/genome sequencing in the cohort.

Subject's ID	Sequencing approach, with reference
1-3	trio WES [28]
4	trio WGS [29,30]
5, 12	trio WES [31]
6	trio WGS [32]
7	singleton WES [33]
8, 15	trio WES [34]
9	trio WES [35]
10	singleton WES [36]
11	trio WES [37]
13	trio WES [38]
14	trio WES [39]
16	trio WES [40]
17	trio WES [41]

Table S2 - Auxological parameters and additional clinical and genetic findings of the 17 individuals with *TMEM63B* variants

Individual number/gender	***TMEM63B* variant (abbreviated form)**	**Weight, length, and head circumference (percentiles), at birth and subsequent follow-up**	**Hearing evaluation (age of formal test where available)**	**Additional clinical findings including haematological haematological manifestations**	**Additional genetic findings**
1/M	V44M	W 3-15th, L<3rd, HC 25-50th; 2y: W <3rd, L 50th, HC 25-50th	8y: normal BAEPS	6m: mild anaemia, mildly increased PLT count, stable on yearly FBC; OFT negative	No other clinically relevant variants
2/M	R433H	W 15-50th, L 15-50th, HC 15-50th; 10y: W <3rd, L >95th, HC 8th	10y: normal BAEPS and audiometric test	6y: high Hb level, 10y: mild abnormalities of RBC, MCV, MCH, no anaemia; OFT negative	No other clinically relevant variants
3/M	T481N	NA	2y: normal audiometric test	None	No other clinically relevant variants
4/M	V44M	W 91-98th, HC 91-98th; 9y: W 50th	4-5w: normal AOAE; no concerns from parents or professionals about individual's hearing (able to respond to auditory stimuli)	Jaundice at birth, then intermittent throughout life but less prominent. From 12m: macrocytic anaemia (leukoerythroblastic picture with nucleated red cells and myelocytes), borderline monocytosis, hepatosplenomegaly. 5y: cholecystectomy for chronic cholecystitis, liver biopsy showed haemosiderin deposits. From 7y: persistent macrocytic anaemia with reticulocytosis, increased stomatocytes, iron deficiency anaemia. From 8y: recurrent chest infections. 10y: RCMO onset (flare-up of osteomyelitis associated with Hb reduction and alopecia patches). From age 10y: transfusion dependent (monthly), severe anaemia, BM: increased RBC production (due to haemolysis), EMA binding test normal, blood film suggested hereditary elliptocytosis, negative genetic test for hereditary spherocytosis	No other clinically relevant variants
5/M	V44M	W 25-50th; 5y: HC 10th; 7y: W 1st, L 30th	No clinical concerns of hearing impairment; no formal hearing test	Jaundice at birth; laryngomalacia (supraglottoplasty at 1y)	No other clinically relevant variants
6/F	V44M	W >99th; 14m: W >99th, L >99th	No clinical concerns of hearing impairment; no formal hearing test	From birth: unexplained macrocytic anaemia, EMA-test analysis normal, haemoglobinopathy screen normal, haemolysis screen negative, negative red cell anaemia TGP, mild hepatosplenomegaly, required transfusion. From 4m to 7m: jaundice. Pharyngomalacia and severe OSA leading to respiratory failure and NIV requirement, recurrent chest infections	No other clinically relevant variants

7/M	V44M	W 60th, L 44th, HC 35th; 20m: W 75th, L >90th, HC 25-50th	3w: normal AOAE	From 12m: scleralicterus	No other clinically relevant variants
8/F	V44M	W 15-50th, L 85-97th, HC 50-85th; 17y: W<5th, L<5th	7 and 10y: normal BAEPs	From 2y: severe anaemia, occasional transfusions, episode of haemolysis triggered by infection. 8y BM showed myelodysplastic syndrome with aplastic anaemia, haematopoiesis, and chronic haemolysis	No other clinically relevant variants
9/M	V44M	W 50th, L 60th, HC 35th; 1y: HC <5th; 10y W 60th; 15y: W <5th, HC <5th	No clinical concerns of hearing impairment; no formal hearing test	Mild and stable anaemia noticed since age 2y (no previous measurement available); retinal dystrophy	*de novo CBL* NM_005188.3:c.1110A>C p.(Leu370Phe); classified as VUS with uncertain contribute to the phenotype (developmental delay)
10/F	D459E	W 62nd, L<3rd HC 83rd; 3y: W 45th, L 73rd, HC 10-25th	No formal hearing test performed, but clinical concern for poor hearing	Fraternal twin, preterm labor, pre-eclampsia, gestational diabetes, pulmonary valve stenosis, hyperbilirubinemia, 2.5y: mild macrocytic anaemia; OFT negative	No other clinically relevant variants
11/M	V463I	W 25-50th; L 25-50th; HC 50-75th; 4y: W 31st, L 23rd; HC 33rd	No clinical concerns of hearing impairment; no formal hearing test	None	No other clinically relevant variants
12/M	V463I	W 25-50th; L 76th; HC 20th; 2y: W 75th; L 59th; HC >99th (+3.43 SD)	1w: normal AOAE	None	*de novo TSC1* NM_000368.5:c.1498C>T p.(Arg500*); described by van Slegtenhorst et al 1999[42]; classified as pathogenic and thought to contribute to the phenotype (macrocephaly)
13/F	I475del	W 3-5th, L 25-50th, HC <3rd; 12y: HC <5th; 16y: W <5th, L<5th	9m: normal BAEPs	From birth, severe haemolytic anaemia with macrocytosis, thrombocytopenia and hepatosplenomegaly, transfusion dependent, hyperbilirubinemia (total bilirubin 37 µmol/l, direct bilirubin 7 µmol/l), left vesicoureteral reflux (surgical correction 13y), chronic urinary retention	No other clinically relevant variants
14/M	G580S	W 50th, L 50th, HC 50th; 4.5y: W <3rd, L<3rd, HC<3rd	No clinical concerns of hearing impairment; no formal hearing test	None	No other clinically relevant variants
15/F	G580C	W 15-50th, L <3rd, HC 15-50th; 15y: W 5-10th, L <5th, HC 50-75th	27y: abnormal BAEPs (left ear: disappearance of II to V waves; right ear: disappearance of II to IV waves and latency prolongation of V wave).	Slight bilirubin increase	No other clinically relevant variants

16/F	R660T	W 50-75th, L 90-95th; 23m: W >97th, L 50-75th, HC >97th	Failed newborn AOAE on the left ear; clinical concern for mid hearing loss; 1y, 11m: AOAE inconclusive; tympanometric tests showed normal middle ear function bilaterally	Birth: mild jaundice, macrocytic anaemia, out-turned feet	arr[GRCh38/hg38] 20p13(391190_508758)x3; classified as VOUS
17/M	F697L	W<3rd; 15y W<3rd, L<3rd	9y: normal audiometric test	None	Maternally inherited *GCK* NM_000162.5:c.107G>A p.(Arg36Gln); described by Osbak et al, 2009[43] - risk factor for type 2 diabetes, reported as unsolicited finding[#]

Additional genetic findings, where reported, were classified according to the ACMG guidelines.[44,45] A comment is provided to illustrate whether the variants is thought to have contributed to the observed phenotype. Abbreviations and symbols: AOAE, automated otoacoustic emission test; BAEPs, brainstem auditory evoked potentials; BM, bone marrow; RCMO, recurrent chronic multifocal osteomyelitis; EMA, eosin-5′-maleimide-binding; F, female; FBC, full blood count; Hb, haemoglobin; HC, head circumference; L, length; M, male; m, months; MCH, mean corpuscular haemoglobin; MCV, mean corpuscular volume; m, months; NA, not available/not applicable; NIV, non-invasive ventilation; OFT, osmotic fragility test; OSA, obstructive sleep apnoea; PLT, platelets; RBC, red blood cells; TGP, targeted gene panel; VUS, variant of uncertain significance; W, weight; w, weeks; y, years; [#]No family members with type 2 diabetes at the time of WES; increased glucose levels in the mother during the pregnancy.

Table S3 - Genomic coordinates and in-silico analysis of the *TMEM63B* variants in our cohort

ID	Variant (genomic GRCh37/hg19)	Protein Change	Exon	GnomAD (v2.1)	TOPMed (Freeze 8)	CADD	SIFT/score	Polyphen-2/score	MutationTaster/score	PhyloP100way	GERP++	Grantham score	Tolerance Score (dN/dS, Metadome)
1, 4-9	6:g.44102451G>A	V44M	2	.	.	26.6	deleterious/0	probably_damaging/0.999	disease_causing/0.99	9.23	4.23	21	0.42
2	6:g.44116567G>A	R433H	15	.	.	29.1	deleterious/0	probably_damaging/0.934	disease_causing/0.99	7.73	4.23	29	0.31
3	6:g.44117624C>A	T481N	16	.	.	25.7	deleterious/0	probably_damaging/0.992	disease_causing/1	7.59	4.48	65	0.08
10	6:g.44116646C>G	D459E	15	.	.	24.5	deleterious/0	probably_damaging/0.943	disease_causing/0.99	3.86	4.48	45	0.15
11-12	6:g.44116656G>A	V463I	15	.	.	26.5	deleterious/0	possibly_damaging/0.85	disease_causing/0.99	9.52	4.48	29	0.16
13	6:g.44117600CCAT>C	I475del	16	.	.	NA	NA	NA	disease_causing/1	7.31	4.48	NA	0.11
14	6:g.44119647G>A	G580S	19	.	.	31	deleterious/0	probably_damaging/0.999	disease_causing/1	9.58	5.01	56	0.14
15	6:g.44119647G>T	G580C	19	.	.	32	deleterious/0	probably_damaging/1	disease_causing/1	10	5.01	159	0.14
16	6:g.44121449G>C	R660T	21	.	.	26.6	deleterious/0	probably_damaging/0.955	disease_causing/0.99	9.26	4.59	71	0.31
17	6:g.44121559T>C	F697L	21	.	.	30	deleterious/0	probably_damaging/0.968	disease_causing/0.99	7.52	4.62	22	0.06

The table shows the coordinates of the variants according to the recommendations of the Human Genome Variation Society (http://varnomen.hgvs.org/), based on the hGRCh37/hg19 assembly and the NM_018426.3 reference transcript. None of the variants was reported in publicly available allele frequency databases such as GnomAD (v2.1) and TOPMed (Freeze 8). For all the variants in our cohort we report the *in-silico* predictions of pathogenicity obtained from multiple tools: for CADD (Combined Annotation-

Dependent Depletion) the PHRED-like scaled C-score greater or equal 20 indicates the 1% most deleterious substitutions to the gene products;[46] SIFT confidence score for a missense variant is computed as 1-p where p is the probability for the variant to be deleterious [47]; for MutationTaster a value close to 1 indicates a high 'security' of the prediction, while for Polyphen-2 it represents the probability for the variant to be disease causing in a 0-1 range) [48]. PhyloP100way and GERP++ scores range from -14.1 to 6.4 and -12.3 to 6.17 respectively, with higher scores indicating stronger constraint.[5,6] Grantham score ranges from 5 to 215 and predicts the distance between two amino acids, in an evolutionary sense. Higher Grantham scores are considered more deleterious.[49] Tolerance Scores (dN/dS nonsynonymous over synonymous ratio according to Metadome) range from highly intolerant (0-0.19) to intolerant (0.2-0.49).[7] NA: not available/not applicable.

Table S4 – Structural analysis of the *TMEM63B* variants by Consurf and Missense3D

ID	Protein Change	Transmembrane domain	Protein domain (Pfam 35.0)	ConSurf scale/prediction	Missense3D prediction
1, 4-9	V44M	TM1	NA	9/predicted structural residue (highly conserved and buried)	Expansion of cavity volume by 8.208 Å^3
2	R433H	TM4	PF02714	8/buried residue	Contraction of cavity volume by 3.888 Å^3
3	T481N	TM5	PF02714	9/predicted structural residue (highly conserved and buried)	No structural damage detected; Unable to calculate cavity in mutant structure
10	D459E	TM4	PF02714	8/predicted functional residue (highly conserved and exposed)	Buried salt bridge breakage (Asp 459, LYS 460)
11, 12	V463I	TM4	PF02714	8/buried residue	Contraction of cavity volume by 13.824 Å^3
13	I475del	TM5	PF02714	5/buried residue	NA
14	G580S	TM7	PF02714	9/predicted structural residue (highly conserved and buried)	Buried Gly residue (RSA 5.9%) replaced with a buried Ser residue (RSA 3.8%); Contraction of cavity volume by 52.056 Å^3
15	G580C	TM7	PF02714	9/predicted structural residue (highly conserved and buried)	Buried Gly residue (RSA 5.9%) replaced with a buried Cys residue (RSA 3.7%); Contraction of cavity volume by 66.744 Å^3
16	R660T	TM8	PF02714	8/predicted functional residue (highly conserved and exposed)	Buried charge replaced (Arg, RSA 5.6%) with an uncharged residue (Thr); Buried salt bridge breakage (Arg 660, Asp 137); Expansion of cavity volume by 60.696 Å^3
17	F697L	TM9	PF02714	8/buried residue	Expansion of cavity volume by 30.24 Å^3

All the affected residues map in a transmembrane (TM) domain, and all but the recurrent V44M are in the RSN1_7TM (PF02714) domain.[50] For all the affected residues, we report the conservation scale (ranging from variable, 1 to conserved, 9) and the neural-network algorithm prediction from ConSurf (https://consurf.tau.ac.il/).[15] For all missense variants, we also show the prediction of possible structural changes according to Missense3D-DB, which considered 17 structural features, including secondary structure alterations, non-covalent bond breakages, and buried residues changes.[16] NA: not available/not applicable.

Supplemental References

1. Li, H., and Durbin, R. (2009). Fast and accurate short read alignment with Burrows-Wheeler transform. Bioinformatics *25*, 1754–1760. 10.1093/bioinformatics/btp324.
2. DePristo, M.A., Banks, E., Poplin, R., Garimella, K. V., Maguire, J.R., Hartl, C., Philippakis, A.A., del Angel, G., Rivas, M.A., Hanna, M., et al. (2011). A framework for variation discovery and genotyping using next-generation DNA sequencing data. Nat. Genet. *43*, 491–498. 10.1038/ng.806.
3. Lek, M., Karczewski, K.J., Minikel, E. V., Samocha, K.E., Banks, E., Fennell, T., O'Donnell-Luria, A.H., Ware, J.S., Hill, A.J., Cummings, B.B., et al. (2016). Analysis of protein-coding genetic variation in 60,706 humans. Nature. 10.1038/nature19057.
4. Liu, X., Jian, X., and Boerwinkle, E. (2011). dbNSFP: a lightweight database of human nonsynonymous SNPs and their functional predictions. Hum. Mutat. *32*, 894–899. 10.1002/humu.21517.
5. Cooper, G.M., Stone, E.A., Asimenos, G., Green, E.D., Batzoglou, S., and Sidow, A. (2005). Distribution and intensity of constraint in mammalian genomic sequence. Genome Res. *15*, 901–913. 10.1101/gr.3577405.
6. Pollard, K.S., Hubisz, M.J., Rosenbloom, K.R., and Siepel, A. (2010). Detection of nonneutral substitution rates on mammalian phylogenies. Genome Res. *20*, 110–121. 10.1101/gr.097857.109.
7. Wiel, L., Baakman, C., Gilissen, D., Veltman, J.A., Vriend, G., and Gilissen, C. (2019). MetaDome: Pathogenicity analysis of genetic variants through aggregation of homologous human protein domains. Hum. Mutat. *40*, humu.23798. 10.1002/humu.23798.
8. Traynelis, J., Silk, M., Wang, Q., Berkovic, S.F., Liu, L., Ascher, D.B., Balding, D.J., and Petrovski, S. (2017). Optimizing genomic medicine in epilepsy through a gene-customized approach to missense variant interpretation. Genome Res. *27*, 1715–1729. 10.1101/gr.226589.117.
9. Sayers, E.W., Bolton, E.E., Brister, J.R., Canese, K., Chan, J., Comeau, D.C., Connor, R., Funk, K., Kelly, C., Kim, S., et al. (2022). Database resources of the national center for biotechnology information. Nucleic Acids Res. *50*. 10.1093/nar/gkab1112.
10. Sievers, F., Wilm, A., Dineen, D., Gibson, T.J., Karplus, K., Li, W., Lopez, R., McWilliam, H., Remmert, M., Söding, J., et al. (2011). Fast, scalable generation of high-quality protein multiple

sequence alignments using Clustal Omega. Mol. Syst. Biol. *7*. 10.1038/msb.2011.75.

11. Kelley, L.A., Mezulis, S., Yates, C.M., Wass, M.N., and Sternberg, M.J.E. (2015). The Phyre2 web portal for protein modeling, prediction and analysis. Nat. Protoc. *10*. 10.1038/nprot.2015.053.

12. Schymkowitz, J., Borg, J., Stricher, F., Nys, R., Rousseau, F., and Serrano, L. (2005). The FoldX web server: An online force field. Nucleic Acids Res. *33*. 10.1093/nar/gki387.

13. Guerois, R., Nielsen, J.E., and Serrano, L. (2002). Predicting changes in the stability of proteins and protein complexes: A study of more than 1000 mutations. J. Mol. Biol. *320*. 10.1016/S0022-2836(02)00442-4.

14. Jumper, J., Evans, R., Pritzel, A., Green, T., Figurnov, M., Ronneberger, O., Tunyasuvunakool, K., Bates, R., Žídek, A., Potapenko, A., et al. (2021). Highly accurate protein structure prediction with AlphaFold. Nature *596*. 10.1038/s41586-021-03819-2.

15. Meier, A., and Söding, J. (2015). Automatic Prediction of Protein 3D Structures by Probabilistic Multi-template Homology Modeling. PLoS Comput. Biol. *11*. 10.1371/journal.pcbi.1004343.

16. Ittisoponpisan, S., Islam, S.A., Khanna, T., Alhuzimi, E., David, A., and Sternberg, M.J.E. (2019). Can Predicted Protein 3D Structures Provide Reliable Insights into whether Missense Variants Are Disease Associated? J. Mol. Biol. *431*. 10.1016/j.jmb.2019.04.009.

17. Pettersen, E.F., Goddard, T.D., Huang, C.C., Couch, G.S., Greenblatt, D.M., Meng, E.C., and Ferrin, T.E. (2004). UCSF Chimera - A visualization system for exploratory research and analysis. J. Comput. Chem. *25*. 10.1002/jcc.20084.

18. Du, H., Ye, C., Wu, D., Zang, Y.Y., Zhang, L., Chen, C., He, X.Y., Yang, J.J., Hu, P., Xu, Z., et al. (2020). The Cation Channel TMEM63B Is an Osmosensor Required for Hearing. Cell Rep. *31*. 10.1016/j.celrep.2020.107596.

19. Sugie, A., Möhl, C., Hakeda-Suzuki, S., Matsui, H., Suzuki, T., and Tavosanis, G. (2017). Analyzing synaptic modulation of drosophila melanogaster photoreceptors after exposure to prolonged light. J. Vis. Exp. *2017*. 10.3791/55176.

20. Groth, A.C., Fish, M., Nusse, R., and Calos, M.P. (2004). Construction of transgenic Drosophila by using the site-specific integrase from phage phiC31. Genetics *166*, 1775–1782. 10.1534/genetics.166.4.1775.

21. Kramer, J.M., and Staveley, B.E. (2003). GAL4 causes developmental defects and apoptosis when expressed in the developing eye of Drosophila melanogaster. Genet. Mol. Res. *2*.

22. Iyer, J., Wang, Q., Le, T., Pizzo, L., Grönke, S., Ambegaokar, S.S., Imai, Y., Srivastava, A., Troisí, B.L., Mardon, G., et al. (2016). Quantitative Assessment of Eye Phenotypes for Functional Genetic Studies Using *Drosophila melanogaster*. G3 Genes|Genomes|Genetics *6*, 1427–1437. 10.1534/g3.116.027060.

23. Hou, C., Tian, W., Kleist, T., He, K., Garcia, V., Bai, F., Hao, Y., Luan, S., and Li, L. (2014). DUF221 proteins are a family of osmosensitive calcium-permeable cation channels conserved across eukaryotes. Cell Res. *24*. 10.1038/cr.2014.14.

24. Yan, H., Helman, G., Murthy, S.E., Ji, H., Crawford, J., Kubisiak, T., Bent, S.J., Xiao, J., Taft, R.J., Coombs, A., et al. (2019). Heterozygous Variants in the Mechanosensitive Ion Channel TMEM63A Result in Transient Hypomyelination during Infancy. Am. J. Hum. Genet. *105*, 996–1004. 10.1016/j.ajhg.2019.09.011.

25. Tonduti, D., Mura, E., Masnada, S., Bertini, E., Aiello, C., Zini, D., Parmeggiani, L., Cantalupo, G., Talenti, G., Veggiotti, P., et al. (2021). Spinal cord involvement and paroxysmal events in "Infantile Onset Transient Hypomyelination" due to TMEM63A mutation. J. Hum. Genet. *66*, 1035–1037. 10.1038/s10038-021-00921-1.

26. Fukumura, S., Hiraide, T., Yamamoto, A., Tsuchida, K., Aoto, K., Nakashima, M., and Saitsu, H. (2022). A novel de novo TMEM63A variant in a patient with severe hypomyelination and global developmental delay. Brain Dev. *44*, 178–183. 10.1016/j.braindev.2021.09.006.

27. Gaublomme, J.T., Li, B., McCabe, C., Knecht, A., Yang, Y., Drokhlyansky, E., Van Wittenberghe, N., Waldman, J., Dionne, D., Nguyen, L., et al. (2019). Nuclei multiplexing with barcoded antibodies for single-nucleus genomics. Nat. Commun. *10*. 10.1038/s41467-019-10756-2.

28. Vetro, A., Nielsen, H.N., Holm, R., Hevner, R.F., Parrini, E., Powis, Z., Møller, R.S., Bellan, C., Simonati, A., Lesca, G., et al. (2021). ATP1A2-and ATP1A3-associated early profound epileptic encephalopathy and polymicrogyria. Brain *144*. 10.1093/brain/awab052.

29. Wright, C.F., Fitzgerald, T.W., Jones, W.D., Clayton, S., McRae, J.F., Van Kogelenberg, M., King, D.A., Ambridge, K., Barrett, D.M., Bayzetinova, T., et al. (2015). Genetic diagnosis of developmental

disorders in the DDD study: A scalable analysis of genome-wide research data. Lancet *385*. 10.1016/S0140-6736(14)61705-0.

30. Fitzgerald, T.W., Gerety, S.S., Jones, W.D., Van Kogelenberg, M., King, D.A., McRae, J., Morley, K.I., Parthiban, V., Al-Turki, S., Ambridge, K., et al. (2015). Large-scale discovery of novel genetic causes of developmental disorders. Nature *519*. 10.1038/nature14135.

31. Dias, K.-R., Carlston, C.M., Blok, L.E.R., De Hayr, L., Nawaz, U., Evans, C.-A., Bayrak-Toydemir, P., Htun, S., Zhu, Y., Ma, A., et al. (2022). De Novo ZMYND8 variants result in an autosomal dominant neurodevelopmental disorder with cardiac malformations. Genet. Med. *24*, 1952–1966. 10.1016/j.gim.2022.06.001.

32. Genomes-Project-Pilot-Investigators, T. (2022). 100,000 genomes pilot on rare-disease diagnosis in health care – preliminary report. Yearb. Paediatr. Endocrinol. 10.1530/ey.19.15.16.

33. Brunet, T., Jech, R., Brugger, M., Kovacs, R., Alhaddad, B., Leszinski, G., Riedhammer, K.M., Westphal, D.S., Mahle, I., Mayerhanser, K., et al. (2021). De novo variants in neurodevelopmental disorders—experiences from a tertiary care center. Clin. Genet. *100*. 10.1111/cge.13946.

34. Sakamoto, M., Iwama, K., Sekiguchi, F., Mashimo, H., Kumada, S., Ishigaki, K., Okamoto, N., Behnam, M., Ghadami, M., Koshimizu, E., et al. (2021). Novel EXOSC9 variants cause pontocerebellar hypoplasia type 1D with spinal motor neuronopathy and cerebellar atrophy. J. Hum. Genet. *66*. 10.1038/s10038-020-00853-2.

35. Terhal, P.A., Vlaar, J.M., Middelkamp, S., Nievelstein, R.A.J., Nikkels, P.G.J., Ross, J., Créton, M., Bos, J.W., Voskuil-Kerkhof, E.S.M., Cuppen, E., et al. (2020). Biallelic variants in POLR3GL cause endosteal hyperostosis and oligodontia. Eur. J. Hum. Genet. *28*. 10.1038/s41431-019-0427-0.

36. Retterer, K., Juusola, J., Cho, M.T., Vitazka, P., Millan, F., Gibellini, F., Vertino-Bell, A., Smaoui, N., Neidich, J., Monaghan, K.G., et al. (2016). Clinical application of whole-exome sequencing across clinical indications. Genet. Med. *18*, 696–704. 10.1038/gim.2015.148.

37. Giacomini, T., Scala, M., Nobile, G., Severino, M., Tortora, D., Nobili, L., Accogli, A., Torella, A., Capra, V., Mancardi, M.M., et al. (2022). De novo POLR2A p.(Ile457Thr) variant associated with early-onset encephalopathy and cerebellar atrophy: expanding the phenotypic spectrum. Brain Dev. *44*, 480–485. 10.1016/j.braindev.2022.04.002.

38. Bergant, G., Maver, A., Lovrecic, L., Čuturilo, G., Hodzic, A., and Peterlin, B. (2018). Comprehensive use of extended exome analysis improves diagnostic yield in rare disease: A retrospective survey in 1,059 cases. Genet. Med. *20*, 303–312. 10.1038/gim.2017.142.

39. Larcher, L., Norris, J.W., Lejeune, E., Buratti, J., Mignot, C., Garel, C., Keren, B., Schwartz, C.E., and Whalen, S. (2020). The complete loss of function of the SMS gene results in a severe form of Snyder-Robinson syndrome. Eur. J. Med. Genet. *63*. 10.1016/j.ejmg.2019.103777.

40. Satterstrom, F.K., Kosmicki, J.A., Wang, J., Breen, M.S., De Rubeis, S., An, J.Y., Peng, M., Collins, R., Grove, J., Klei, L., et al. (2020). Large-Scale Exome Sequencing Study Implicates Both Developmental and Functional Changes in the Neurobiology of Autism. Cell *180*. 10.1016/j.cell.2019.12.036.

41. de Koning, M.A., Hoffer, M.J.V., Nibbeling, E.A.R., Bijlsma, E.K., Toirkens, M.J.P., Adama-Scheltema, P.N., Verweij, E.J., Veenhof, M.B., Santen, G.W.E., and Peeters-Scholte, C.M.P.C.D. (2022). Prenatal exome sequencing: A useful tool for the fetal neurologist. Clin. Genet. *101*. 10.1111/cge.14070.

42. Van Slegtenhorst, M., Verhoef, S., Tempelaars, A., Bakker, L., Wang, Q., Wessels, M., Bakker, R., Nellist, M., Lindhout, D., Halley, D., et al. (1999). Mutational spectrum of the TSC1 gene in a cohort of 225 tuberous sclerosis complex patients: No evidence for genotype-phenotype correlation. J. Med. Genet. *36*. 10.1136/jmg.36.4.285.

43. Osbak, K.K., Colclough, K., Saint-Martin, C., Beer, N.L., Bellanné-Chantelot, C., Ellard, S., and Gloyn, A.L. (2009). Update on mutations in glucokinase (GCK), which cause maturity-onset diabetes of the young, permanent neonatal diabetes, and hyperinsulinemic hypoglycemia. Hum. Mutat. *30*. 10.1002/humu.21110.

44. Richards, S., Aziz, N., Bale, S., Bick, D., Das, S., Gastier-Foster, J., Grody, W.W., Hegde, M., Lyon, E., Spector, E., et al. (2015). Standards and guidelines for the interpretation of sequence variants: A joint consensus recommendation of the American College of Medical Genetics and Genomics and the Association for Molecular Pathology. Genet. Med. *17*. 10.1038/gim.2015.30.

45. Riggs, E.R., Andersen, E.F., Cherry, A.M., Kantarci, S., Kearney, H., Patel, A., Raca, G., Ritter, D.I., South, S.T., Thorland, E.C., et al. (2020). Technical standards for the interpretation and reporting of

constitutional copy-number variants: a joint consensus recommendation of the American College of Medical Genetics and Genomics (ACMG) and the Clinical Genome Resource (ClinGen). Genet. Med. *22*. 10.1038/s41436-019-0686-8.

46. Rentzsch, P., Witten, D., Cooper, G.M., Shendure, J., and Kircher, M. (2019). CADD: predicting the deleteriousness of variants throughout the human genome. Nucleic Acids Res. *47*, D886–D894. 10.1093/nar/gky1016.

47. Kumar, P., Henikoff, S., and Ng, P.C. (2009). Predicting the effects of coding non-synonymous variants on protein function using the SIFT algorithm. Nat. Protoc. *4*, 1073–1081. 10.1038/nprot.2009.86.

48. Adzhubei, I.A., Schmidt, S., Peshkin, L., Ramensky, V.E., Gerasimova, A., Bork, P., Kondrashov, A.S., and Sunyaev, S.R. (2010). A method and server for predicting damaging missense mutations. Nat. Methods *7*, 248–249. 10.1038/nmeth0410-248.

49. Grantham, R. (1974). Amino acid difference formula to help explain protein evolution. Science (80-.). *185*. 10.1126/science.185.4154.862.

50. Mistry, J., Chuguransky, S., Williams, L., Qureshi, M., Salazar, G.A., Sonnhammer, E.L.L., Tosatto, S.C.E., Paladin, L., Raj, S., Richardson, L.J., et al. (2021). Pfam: The protein families database in 2021. Nucleic Acids Res. *49*. 10.1093/nar/gkaa913.